International Journal for Multidisciplinary Research (IJFMR)
E-ISSN: 2582-2160 ● Website: www.ijfmr.com ● Email: editor@ijfmr.com

Structure and Optical Properties of Calcium Titanates Perovskite doped with Er^{3+}/Yb^{3+} and $Er^{3+}/Yb^{3+}/Nd^{3+}$ ions

Anshu Singh[1], Preeti Gupta[2]

[1]Research Scholar, Department of Chemistry, DDU Gorakhpur University, Gorakhpur
[2]Assistant Professor, Department of Chemistry, DDU Gorakhpur University, Gorakhpur

Abstract
Calcium Titanates doped with trivalent Er, Er/Yb, and Er/Yb/Nd ions have been prepared by solid-state route. XRD patterns are recorded for materials and the Rietveld structural analysis shows orthorhombic crystal structure with space group *Pbnm*. The HRSEM image of undoped $CaTiO_3$ and doped material indicate agglomerate of spherical particles. Results obtained from EDS analysis proves the presence of elements i.e. Ca, Er, Yb, Nd, Ti and O in the phosphor material with appropriate compositional homogeneity. The FTIR spectra confirm the characteristic vibrational features of the perovskite lattice. Optical band gap of prepared phosphor materials increases with incorporation of Ln^{3+} ions. Hence, the perovskite phosphors may be very beneficial in solid-state lighting, display devices and white light emitting diodes (LEDs).

Keywords: Solid State Synthesis, Perovskite, Lanthanide ions, Optical band gap, $CaTiO_3$

1. Introduction

The perpetual demand for advanced photonic materials, driven by applications in solid-state lighting, displays, solar energy conversion, and biomedical imaging, has positioned luminescent materials at the forefront of materials science research [1]. Among these, materials exhibiting efficient upconversion (UC) luminescence—the process of converting lower-energy photons into higher-energy light—are particularly valuable, as they enable new functionalities like infrared-pumped visible lasers and deep-tissue imaging probes [2, 3].

A critical determinant of a luminescent material's performance is its host matrix. The perovskite family, with its general formula ABO_3, offers an exceptionally versatile platform due to its structural tolerance to extensive ionic substitutions and its tunable electronic properties [4]. Calcium titanate ($CaTiO_3$), a prototypical perovskite, is an especially attractive host for lanthanide ions. While the ideal perovskite structure is cubic, $CaTiO_3$ crystallizes in an orthorhombic structure (space group *Pbnm*) at room temperature, characterized by tilted TiO_6 octahedra [5]. This low-symmetry environment creates a strong crystal field around dopant ions, which enhances the probability of forced electric dipole transitions in lanthanide activators, leading to intense luminescence [6]. Furthermore, its chemical stability and relatively low maximum phonon energy in the few hundred cm^{-1} range (upto ~440 cm^{-1}) help minimize non-radiative relaxation, thereby preserving the excited-state energy of dopants for efficient light emission [7].

The strategic incorporation of trivalent lanthanide ions (Ln^{3+}) is the primary method for imparting specific optical functions to the $CaTiO_3$ host. However, the practical application of many Ln^{3+} ions is limited by their narrow and weak absorption bands, a consequence of the forbidden nature of 4f-4f transitions [8]. To overcome this, co-doping strategies have been developed, wherein a "sensitizer" ion with a large absorption cross-section transfers its energy to an "activator" ion. The Er^{3+}/Yb^{3+} pair is a paradigm of this approach. Yb^{3+}, with its simple two-level structure ($^2F_{7/2} \rightarrow {}^2F_{5/2}$), efficiently absorbs 980 nm radiation from commercially abundant laser diodes and subsequently transfers the energy to Er^{3+}, populating its excited states and leading to characteristic green ($^2H_{11/2}$, $^4S_{3/2} \rightarrow {}^4I_{15/2}$) and red ($^4F_{9/2} \rightarrow {}^4I_{15/2}$) UC emissions [9, 10]. This energy transfer process can involve multiple photons, making the system highly efficient for UC applications.

To further enhance the versatility and excitation flexibility of these materials, a third ion can be introduced. Neodymium (Nd^{3+}) is an excellent candidate, possessing strong absorption features around 808 nm, another common and biologically friendly laser wavelength [11]. In a tri-doped system ($Er^{3+}/Yb^{3+}/Nd^{3+}$), a synergistic energy transfer cascade can be established: Nd^{3+} acts as a primary absorber at 808 nm, transfers energy to the Yb^{3+} sublattice, which then sensitizes the Er^{3+} activator [12]. This relay mechanism creates a multi-wavelength excitable phosphor, broadening its potential application scope.

While the luminescence of Er^{3+}/Yb^{3+} co-doped systems has been explored in various hosts [9], the detailed photophysical processes in $CaTiO_3$, particularly the impact of its orthorhombic structure on energy transfer efficiencies and the comparative analysis with the tri-doped $Er^{3+}/Yb^{3+}/Nd^{3+}$ system, remain less comprehensively investigated. A systematic study linking the structural properties of the $CaTiO_3$ host to the optical performance of these co-doping schemes is crucial for rational material design.

This work aims to provide a detailed investigation of the structure and optical properties of $CaTiO_3$ perovskites doped with Er^{3+}/Yb^{3+} and $Er^{3+}/Yb^{3+}/Nd^{3+}$ ions. The findings are expected to contribute to the development of efficient, multi-functional luminescent materials for next-generation photonic technologies.

2. Experimental section

2.1. Synthesis of materials

Perovskite phosphors $Ca_{(1-x+y+z)}Er_xYb_yNd_zTiO_3$ have been synthesized by solid state route at 1573 K. Analytical-grade of calcium carbonate ($CaCO_3$, ~98%), Titanium oxide (TiO_2, ~99%) , Erbiium oxide (Er_2O_3, ~99.5%), Yetterbium oxide (Yb_2O_3, ~99.9%) and Neodynium oxide (Nd_2O_3, ~99.9%) were used. Doping of Er^{3+}, Yb^{3+} and Nd^{3+} has been done in host perovskite and the required amounts of oxides were calculated on a per-formula-unit basis $Ca_{(1-x+y+z)}Er_xYb_yNd_zTiO_3$ (where $x Er^{3+}$=0.01, $y Yb^{3+}$=0.01, $z Nd^{3+}$=0.01). The synthesized stoichiometric perovskite material are $CaTiO_3$, $Ca_{0.99}$ $Er_{0.01}TiO_3$, $Ca_{0.98}Er_{0.01}Yb_{0.01}TiO_3$ and $Ca_{0.97}$ $Er_{0.01}Yb_{0.01}Nd_{0.01}TiO_3$). The accurately weighed materials were transferred to an agate mortar, mixed with a few drops of acetone to make a slurry, and manually ground for ≥ 120 min to obtain a homogeneous fine mixture. The resulting mixture is placed in an alumina crucible and heated in air using a programmable furnace. The temperature was ramped to 1573 K at 5 °C min^{-1} and held for 4 h to promote solid-state diffusion and crystallization of the orthorhombic perovskite phase (P*bnm*). After cooling to room temperature, the sintered mixtures were ground to fine powders for structural and optical characterization. All samples were prepared by following the same procedure. This low-cost solid-state synthesis yields phase-pure $CaTiO_3$-based phosphors with the dopants incorporated into the Ca lattice sites, as reported for Er/Yb-co-doped $CaTiO_3$ [13].

2.2. Instrument used

By using FullProf Suite, X-ray diffraction (XRD) data collection and Rietveld structure refinement of the XRD patterns were confirmed the crystallinity and purity of the crystallographic phase [14-16]. The MiniFlex 600 diffractometer, supplied by Rigaku, Japan, was used to gather the XRD data. With the aid of a Nova NanoSEM 450-unit, energy dispersive X-ray spectroscopy (EDS) and high-resolution scanning electron microscopy (HRSEM) were used to analyze the microstructure and elemental distributions, respectively. Using Jasco-V-650 instruments, ultraviolet-visible (UV-Vis) spectroscopic measurements of $Ca_{(1-x+y+z)}Er_xYb_yNd_zTiO_3$ phosphors were captured in the absorbance mode. The $Ca_{(1-x+y+z)}Er_xYb_yNd_zTiO_3$ perovskite phosphors' vibrational bands were clarified by monitoring their Fourier transform infrared (FTIR) spectra with a Shimadzu IR Spirit FT-IR-8000 spectrometer.

3. Result and Discussion

3.1. X-ray Diffraction and Structural Analysis

The phase purity and crystal structure of undoped and rare-earth-doped $CaTiO_3$ (CT) samples were examined by using X-ray diffraction (XRD). Figure 1 displays the diffraction patterns of pure CT and CT doped with Er^{3+}, Er^{3+}/Yb^{3+} and $Er^{3+}/Yb^{3+}/Nd^{3+}$ ions. All observed peaks are well indexed to the orthorhombic perovskite phase of $CaTiO_3$ with space group *Pbnm* (JCPDS card no. 01-088-0790), confirming the formation of a single-phase structure without any impurity reflections. The intense diffraction peaks at approximately $2\theta = 33°$, 47°, and 58° correspond to the (121), (202), and (240) planes, respectively, in good agreement with the standard pattern [17].

No additional peaks were observed after doping. This suggests that Er^{3+}, Yb^{3+}, and Nd^{3+} ions successfully substituted into the Ca^{2+} site within the perovskite lattice without forming secondary phases. A slight shift of diffraction peaks toward higher 2θ values and a minor reduction in intensity were noted with increasing dopant concentration, which can be attributed to lattice distortion arising from the incorporation of smaller trivalent rare-earth ions (Er^{3+} = 0.89 Å, Yb^{3+} = 0.868 Å, Nd^{3+} = 0.983 Å) in place of Ca^{2+} (1.00 Å) [18]. Such substitutions induce localized strain and modify the TiO_6 octahedral environment, slightly affecting the lattice symmetry and cell volume.

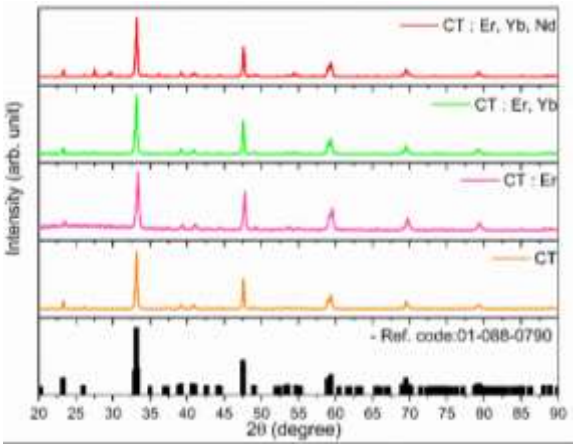

Figure 1 XRD patterns for $CaTiO_3$(CT), $Ca_{0.99}Er_{0.01}TiO_3$ (CT:Er), $Ca_{0.98}Er_{0.01}Yb_{0.01}TiO_3$ (CT:Er^{3+}/Yb^{3+}) and $Ca_{0.97}Er_{0.01}Yb_{0.01}Nd_{0.01}TiO_3$ (CT:$Er^{3+}/Yb^{3+}/Nd^{3+}$) observed at room temperature.

In order to obtain deeper insight into the structural evolution, Rietveld refinement of the XRD data was performed using the FullProf software suite. Figure 2a to 2d shows the refined patterns for pure and doped CT samples, where the observed (Y_{obs}), calculated (Y_{calc}), and difference (Y_{obs}-Y_{calc}) profiles exhibit excellent agreement. The vertical tick marks represent the allowed Bragg positions for the orthorhombic *Pbnm* phase. The low values of residual factors (R_F, R_B) and the goodness-of-fit parameter (χ^2) confirm the reliability of the refinements and the absence of any secondary phases.

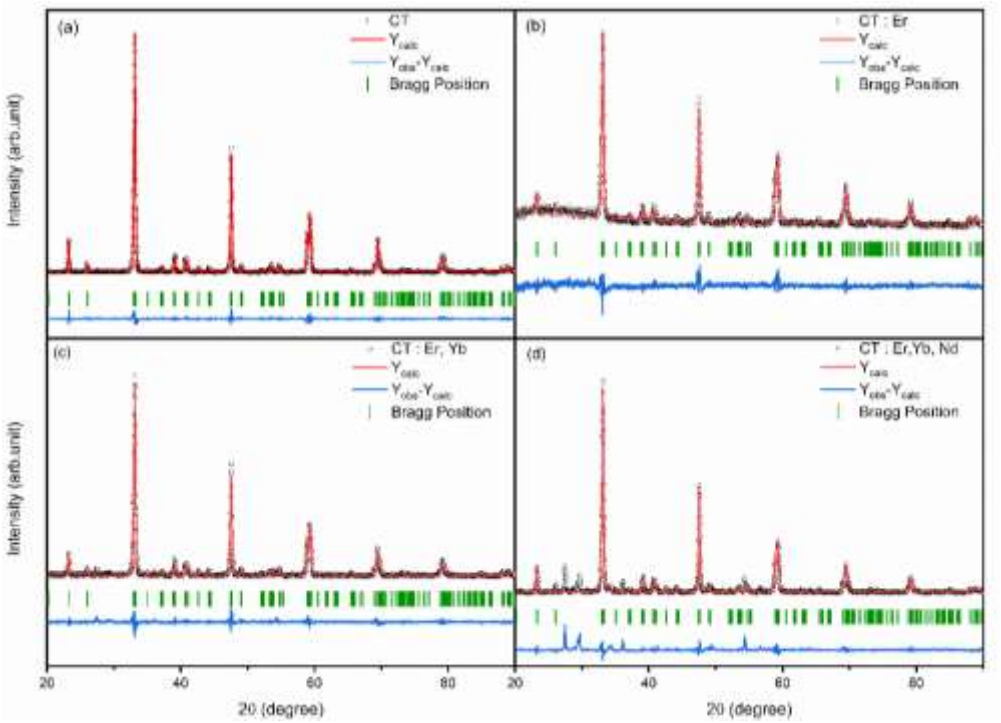

Figure 2 Rietveld fits between the observed and simulated XRD patterns for (a) $CaTiO_3$(CT), (b) $Ca_{0.99}Er_{0.01}TiO_3$ (CT:Er), (c) $Ca_{0.98}Er_{0.01}Yb_{0.01}TiO_3$ (CT:Er^{3+}/Yb^{3+}), and (d) $Ca_{0.97}Er_{0.01}Yb_{0.01}Nd_{0.01}TiO_3$ (CT:Er^{3+}/Yb^{3+}/Nd^{3+}) perovskite phosphors

The refined atomic coordinates, Wyckoff positions, and site occupancies are summarized in Table 1. In all samples, Ca^{2+} occupies the 4c sites, Ti^{4+} resides at the 4b sites, and oxygen atoms are distributed among the 4c and 8d sites-consistent with the orthorhombic perovskite structure [17] (Howard et al., 1989). The partial occupancy values have confirmed the substitution of rare-earth ions at the Ca^{2+} sites (i.e. 0.99 Ca + 0.01 Er for CT:Er^{3+}). This suggests that dopants are successfully incorporated without disrupting the host's framework. The refined lattice constants and unit cell volumes are tabulated in Table 2. The volume increases slightly from 223.8514 Å³ (pure CT) to 224.0104 Å³ (CT co-doped with Er/Yb/Nd). These small increments in cell volume and subtle distortions are indicative of effective lattice accommodation of the dopant ions [19].

The XRD and Rietveld refinement results play a critical role in understanding the luminescence behavior of $CaTiO_3$-based phosphors. The confirmed single-phase orthorhombic perovskite structure ensures minimal non-radiative recombination pathways, which is essential for maintaining high photoluminescence efficiency [20,21].The substitution of Er^{3+}, Yb^{3+}, and Nd^{3+} ions at the Ca^{2+} site modifies the local crystal field and symmetry around the activator ions, influencing the splitting of the 4f energy levels and enhancing both upconversion and downshifting emission processes [1].

Table 1
Refined atomic coordinates (x, y, z), site and occupancy parameters obtained from Rietveld refinement for $Ca_{(1-x+y+z)}Er_xYb_yNd_zTiO_3$.

Atom	Site	Coordinate(x,y,z)	Occupancy
Ca	4c	(0.00848, 0.03570, 0.25000)	1.0Ca
Ti	4b	(0.00000, 0.50000, 0.00000)	1.0
O_1	4c	(0.57840, -0.01577, 0.25000)	1.0
O_2	8d	(0.28783, 0.29025, 0.03392)	2.0
Ca/Er	4c	(0.00752, 0.03434, 0.25000)	0.99Ca + 0.010Er
Ti	4b	(0.00000, 0.50000, 0.00000)	1.0
O_1	4c	(0.56571, -0.01148, 0.25000)	1.0
O_2	8d	(0.29529, 0.28220, 0.04183)	2.0
Ca/Er/Yb	4c	(0.00939, 0.03486, 0.25000)	0.98Ca + 0.010Er +0.010Yb
Ti	4b	(0.00000, 0.50000, 0.00000)	1.0
O_1	4c	(0.58831, -0.02197 0.25000)	1.0
O_2	8d	(0.28738, 0.29105, 0.03090)	2.0
Ca/Er/Yb/Nd	4c	(0.01138, 0.03532, 0.25000)	0.970Ca + 0.010Er +0.010Yb +0.010Nd
Ti	4b	(0.00000, 0.50000, 0.00000)	1.0
O_1	4c	(0.58623, -0.01631, 0.25000)	1.0
O_2	8d	(0.28537, 0.29091, 0.03184)	2.0

Yb^{3+} ions act as effective sensitizers, absorbing near-infrared photons and transferring the energy non-radiatively to Er^{3+} or Nd^{3+} ions, which subsequently emit visible or NIR light. The subtle expansion of the lattice parameters has been mentioned in Table 2. This suggests a reduction in local symmetry and increased phonon coupling, which can facilitate multiphonon relaxation and energy migration between dopant ions [18,21]. Moreover, the absence of impurity phases ensures that all emission centres are well-isolated within the $CaTiO_3$ matrix, resulting in sharp, stable luminescence peaks.

Table 2
Refined lattice parameters (a, b, c) and unit cell volume (V), residual parameters (R_F and R_B) and goodness of fit factor (χ^2) for $Ca_{(1-x+y+z)}Er_xYb_yNd_zTiO_3$ perovskite phosphors.

Phosphors	a(Å)	b(Å)	c(Å)	V(Å^3)	R_F	R_B	χ^2
$CaTiO_3$	5.3827	5.4409	7.6434	223.8514	6.02	5.05	1.528
$Ca_{0.99}$ $Er_{0.01}TiO_3$	5.3807	5.4436	7.6422	223.8432	5.65	4.89	1.801
$Ca_{0.98}Er_{0.01}Yb_{0.01}TiO_3$	5.3837	5.4419	7.6440	223.9532	8.38	8.14	1.45
$Ca_{0.97}$ $Er_{0.01}Yb_{0.01}Nd_{0.01}TiO_3$	5.3849	5.4414	7.6450	224.0104	16.7	11.9	3.037

Therefore, the structural integrity and controlled lattice distortion observed in the Rietveld-refined data demonstrate that $CaTiO_3$ provides a strong and optically favourable environment for rare-earth ion incorporation, making it a promising host lattice for luminescent applications in solid-state lighting and photonic devices.

Figure 3 shows the variation in the unit cell volume with rare-earth substitution. Figure 4(a, b and c) displays a ball and stick unit cell structure model for unit cell of CT, CT:Er, CT:Er,Yb, CT:Er,Yb,Nd perovskite phosphor having orthorhombic crystal structure with P*bnm* space group. Ball and stick unit cell structure model was drawn with the help of VESTA software[22].

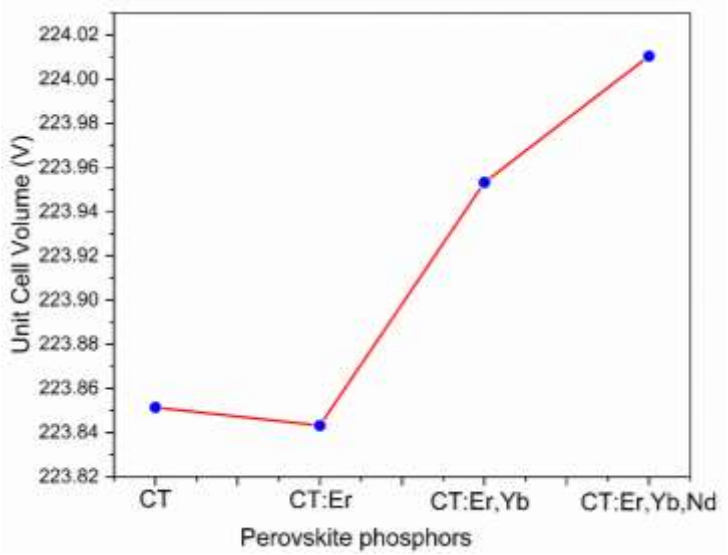

Figure 3 Variation of unit cell volume (V) with CT and $Ca_{(1-x+y+z)}Er_xYb_yNd_zTiO_3$ perovskite phosphors material.

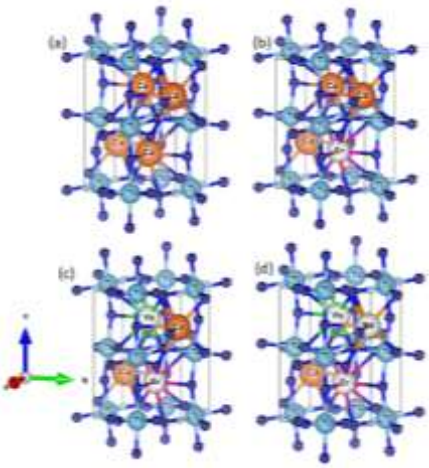

Figure 4 Ball and stick unit cell structural model of (a) CT; (b) CT:Er; (c) CT: Er/Yb; (d) CT:Er/Yb/Nd

3.2. Morphological and Elemental Analysis

The surface morphology and microstructural characteristics of the synthesized $CaTiO_3$ (CT) and rare-earth doped CT phosphors were investigated using high-resolution scanning electron microscopy (HRSEM). Their elemental composition was confirmed through energy-dispersive X-ray spectroscopy (EDX). Figure 5 (a-d) presents the HRSEM micrographs of pure CT, CT:Er^{3+}, CT:Er^{3+}/Yb^{3+}, and CT:Er^{3+}/Yb^{3+}/Nd^{3+} samples along with their corresponding EDX spectra.

The HRSEM images clearly show that all the samples exhibit a nearly homogeneous surface morphology.

The SEM pictures were characterized by agglomerated irregularly shaped grains [19]. The particle sizes lie roughly between 200-500 nm, indicating a polycrystalline nature consistent with the XRD results. Upon doping, a slight increase in grain size and improved surface densification is observed. This may arise because of the incorporation of rare-earth ions at the Ca^{2+} sites. These ions can influence grain boundary mobility, sintering kinetics, promoting particle fusion and enhancing crystallinity [23] (Li et al., 2018). The observed morphology provides a large number of active surface sites, which is beneficial for light-matter interaction and radiative transitions within the luminescent centres.

The corresponding EDX spectra confirm the presence of the expected constituent elements; calcium (Ca), titanium (Ti), and oxygen (O) in all samples, verifying the stoichiometric formation of $CaTiO_3$. Additionally, weak but distinct peaks corresponding to Er, Yb, and Nd ions are visible in the doped samples, validating the successful incorporation of dopant ions within the host lattice. The absence of any foreign or unexpected elements further corroborates the phase purity already established by the XRD and Rietveld analyses.

From the luminescence perspective, the homogeneous microstructure and chemical uniformity that observed in the material plays a crucial role in optimizing the photophysical behaviour of the phosphor. Uniform particle morphology ensures consistent local environments for the activator ions, reducing scattering losses and non-radiative recombination pathways [24] (Zhou et al., 2019). Moreover, well-connected grain boundaries facilitate efficient energy migration between sensitizer (Yb^{3+}) and activator (Er^{3+}/Nd^{3+}) ions, leading to enhanced emission intensity. Thus, the HRSEM and EDX analyses confirm that the synthesized samples possess both structural and compositional integrity, making them suitable for high-performance luminescent applications.

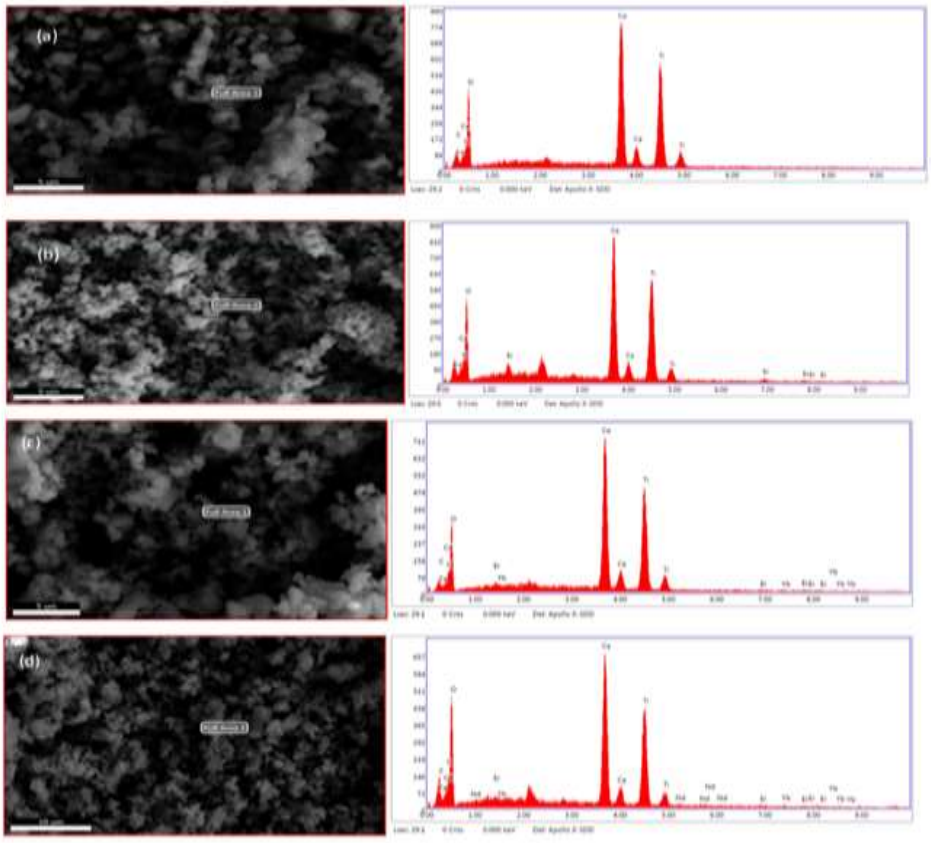

Figure 5 HRSEM micrograph and EDS spectra for the $Ca_{(1-x+y+z)}Er_xYb_yNd_zTiO_3$ perovskite phosphors (a) CT; (b) (b) CT:Er; (c) CT: Er/Yb; (d) CT:Er/Yb/Nd

4. Optical Properties

4.1. FTIR Analysis

The Fourier Transform Infrared (FTIR) transmission spectra of undoped $CaTiO_3$ (CT) and doped samples-CT:Er, CT:Er/Yb, and CT:Er/Yb/Nd are presented in Figure 6. The undoped CT exhibits the highest transmission (~95-100%) across the measured range, indicating a well-ordered perovskite structure with minimal defect-related absorption. In contrast, the doped samples display reduced transmission (increased absorption) in the 400-1000 cm^{-1} region, accompanied by small shoulders and intensity variations. These absorption features correspond to Ti-O-Ti bending vibrations near ~450 cm^{-1} and Ti-O stretching modes around ~560-580 cm^{-1}, which are characteristic of the $CaTiO_3$ lattice [25].

The persistence of the main Ti-O vibrational bands across all doped samples confirms that the host perovskite structure remains intact. The observed shifts and broadening of these bands are indicative of dopant-induced lattice distortion and the formation of local rare-earth-oxygen coordination environments, likely associated with the creation of charge-compensating defects such as oxygen vacancies[26].

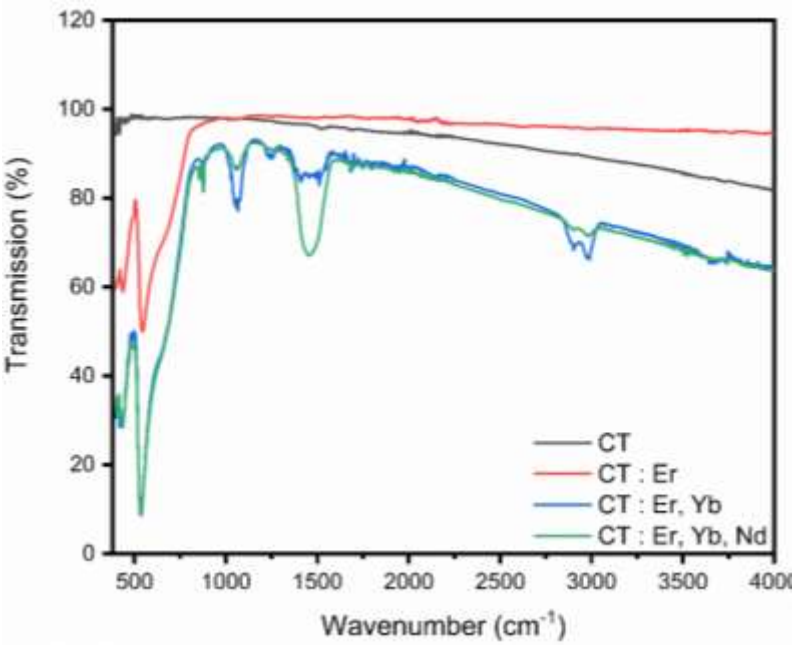

Figure 6 FTIR spectra for the $Ca_{(1-x+y+z)}Er_xYb_yNd_zTiO_3$ perovskite phosphors.

This leads to a broader phonon distribution in the low-wavenumber region (400-900 cm^{-1}). Such modifications increase the density of vibrational states and defect levels that can couple non-radiatively with the excited states of lanthanide ions. This phonon coupling facilitates multiphonon relaxation processes, thereby affecting the luminescence efficiency and decay kinetics [27]. The co-doped samples (CT:Er/Yb and CT:Er/Yb/Nd) exhibit more pronounced broadening and red shifting of the mid-IR Ti–O vibrational bands, indicating increased lattice perturbation and a higher density of defects. These defects can act as non-radiative quenching centers, potentially leading to a reduction in emission intensity and lifetime. Conversely, the closer proximity of ions and modified local crystal fields induced by this lattice distortion may enhance the energy transfer efficiency from the sensitizers (Yb^{3+}/Nd^{3+}) to the activator (Er^{3+}). The net upconversion performance is therefore a result of this balance and is highly dependent on achieving an optimal dopant concentration that maximizes energy transfer while minimizing quenching[28].

Overall, the FTIR results confirm that all dopants are successfully incorporated into the $CaTiO_3$ lattice without the formation of secondary phases, while introducing minimal vibrational modifications that directly influence the optical behaviour. The correlation between enhanced phonon activity observed in FTIR and luminescence characteristics supports the crucial role of host-dopant interactions in determining energy transfer dynamics and emission efficiency in rare-earth doped perovskite phosphors.

4.2. UV-Visible analysis

The optical behavior of the synthesized $CaTiO_3$-based phosphors was investigated through UV-Vis diffuse reflectance spectroscopy (DRS) in the wavelength range of 200-800 nm, as illustrated in Figure 7(a). The reflectance spectra reveal a distinct absorption edge in the UV region, characteristic of the wide bandgap of perovskite oxides. The undoped $CaTiO_3$ (CT) exhibits lower reflectance across the visible region, while Er^{3+}, Yb^{3+}, and Nd^{3+} co-doping significantly enhances the reflectance intensity, particularly in the visible–near infrared (NIR) region. This enhancement is attributed to the incorporation of rare-earth ions, which introduces additional intra-4f electronic transitions and defect-related localized states within the bandgap. These modifications alter the light scattering and absorption properties and can influence the onset of the fundamental charge transfer transition (O 2p → Ti 3d) that defines the bandgap [29].

The corresponding Tauc plots for direct allowed transitions, shown in Figure 7(b), were constructed using the Kubelka-Munk function versus photon energy. The extrapolation of the linear region to the energy axis yields the optical bandgap (E_g) values, which are summarized in Table 3. The pristine $CaTiO_3$ exhibits an E_g of 3.27 eV, which slightly increases upon Er^{3+} and Yb^{3+} doping (3.31and 3.42 eV, respectively). This bandgap widening can be attributed to the substitution of smaller-radius RE^{3+} ions at the Ca^{2+} site, leading to lattice distortion and modified electronic band structures [30]. The incorporation of Nd^{3+}ions in Er-Yb co-doped compositions further increases the E_g (3.43 eV), suggesting improved structural rigidity and reduced defect states within the lattice.

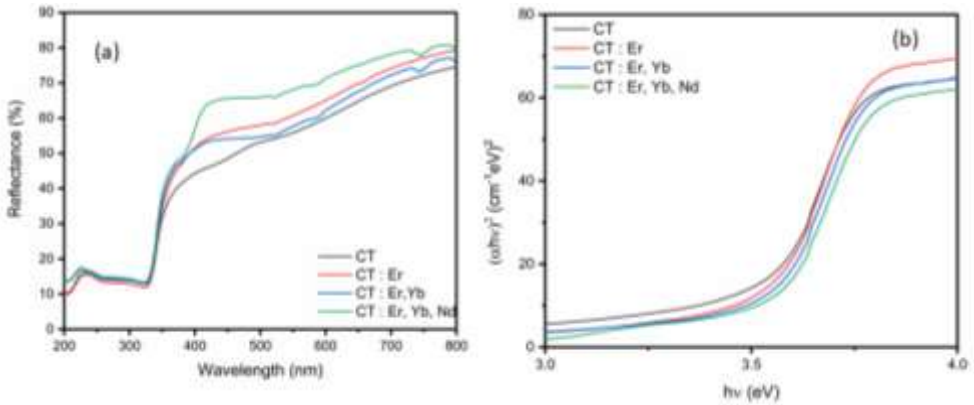

Figure 7 (a) UV-vis absorbance spectra of $Ca_{(1-x)}Er_xTiO_3$ powders; (b) Optical band gap for $Ca_{(1-x+y+z)}Er_xYb_yNd_zTiO_3$ perovskite

Table 3

Optical band gap (Eg) for $Ca_{(1-x+y+z)}Er_xYb_yNd_zTiO_3$ perovskite phosphor materials.

Phosphors	Eg(eV)
$CaTiO_3$	3.2777
$Ca_{0.99}Er_{0.01}TiO_3$	3.3105
$Ca_{0.98}Er_{0.01}Yb_{0.01}TiO_3$	3.4158

$Ca_{0.97}Er_{0.01}Yb_{0.01}Nd_{0.01}TiO_3$	3.4320

From a luminescence perspective, the observed bandgap tuning plays a crucial role in optimizing the excitation-emission processes of the phosphor materials. The slightly increased bandgap upon RE^{3+} co-doping enhances the efficiency of photon absorption in the UV region and facilitates efficient energy transfer between sensitizer-activator pairs such as $Yb^{3+}\rightarrow Er^{3+}$ and $Nd^{3+}\rightarrow Yb^{3+}$. This cooperative sensitization mechanism is vital for upconversion (UC) and down conversion (DC) luminescence processes, enabling multi-photon excitation or energy cascade emission pathways [31] (Wang et al., 2021). Specifically, the increased reflectance and bandgap tuning suggest a reduced probability of nonradiative relaxation and enhanced visible/NIR emission efficiency, making the co-doped $CaTiO_3$:Er^{3+},Yb^{3+},Nd^{3+} system a promising host for luminescent devices and photonic applications. UV-Vis and Tauc analyses confirm that RE^{3+} ion doping effectively modulates the optical bandgap and enhances reflectance, directly impacting luminescent performance through efficient energy transfer dynamics conducive to both upconversion and downconversion mechanisms.

5. Conclusions

Synthesized pure $CaTiO_3$ and doped with Er^{3+}, Er^{3+}/Yb^{3+}, $Er^{3+}/Yb^{3+}/Nd^{3+}$ samples have a single-phase orthorhombic perovskite structure according to XRD examination. The successful substitution of the smaller rare-earth ions into the Ca^{2+} sites, which results in a minor increase in unit cell volume and slight lattice distortion, is confirmed by Rietveld refinement. The structural integrity of the material is guaranteed by the lack of any impurity phases. In order to achieve effective luminescence in this phosphor system, dopants must be carefully incorporated into the host lattice. HRSEM analysis reveals that all $CaTiO_3$ samples have a polycrystalline morphology with agglomerated, irregular grains ranging from 200-500 nm. Doping leads to a slight increase in grain size and improved surface densification. EDX spectra confirm the presence of all expected base elements (Ca, Ti, O) as well as the successful incorporation of the rare-earth dopants (Er, Yb, Nd). This homogeneous microstructure and chemical purity are essential for efficient luminescence. FTIR analysis confirms the successful incorporation of dopants into the $CaTiO_3$ lattice, revealing dopant-induced lattice distortions and increased phonon coupling that influence luminescence efficiency. UV-Vis spectroscopy shows that doping increases the material's reflectance and widens its optical bandgap. This bandgap tuning enhances UV light absorption and facilitates efficient energy transfer between the rare-earth ions. These optical modifications are crucial for optimizing the upconversion and downconversion luminescence performance.

Reference

1. Blasse, G., Grabmaier, B. C. (1994). Luminescent Materials. Springer-Verlag.
2. Auzel, F., “Upconversion and Anti-Stokes Processes with f and d Ions in Solids”, Chemical Reviews, 2004, 104 (1), 139–174.
3. Haase, M., and Schäfer, H., “Upconverting Nanoparticles”, Angewandte Chemie International Edition, 2011, 50 (26), 5808–5829.
4. Bhalla, A. S., Guo, R., and Roy, R., “The Perovskite Structure—A Review of Its Role in Ceramic Science and Technology”, Materials Research Innovations, 2000, 4 (1), 3–26.
5. Büttner, R. H., and Maslen, E. N., “Structural Parameters and Electron Difference Density in $CaTiO_3$”, Acta Crystallographica Section B, 1992, 48 (6), 764–769.

6. Li, G., Jiang, S., Liu, A., Ye, L., Ke, J., Liu, C., Chen, L., Liu, Y., and Hong, M., "Crystal-Field-Perturbation-Enhanced Luminescence of Lanthanide-Doped Nanocrystals through Interstitial H^+ Doping", Nature Communications, 2023, 14 (1), 5870.
7. Mazzo, T., Oliveira, L., Macario, L., Filho, W. R., Andre, R., Rosa, I., Varela, J., and Longo, E., "Photoluminescence Properties of $CaTiO_3$ Phosphors Doped with Eu^{3+} and Tb^{3+} Obtained by the Polymeric Precursor Method", Materials Chemistry and Physics, 2014, 145 (1–2), 201–207.
8. Suyver, J. F., Grimm, J., van Veen, M. K., Biner, D., Krämer, K. W., and Güdel, H. U., "Novel Materials Doped with Trivalent Lanthanides and Transition Metal Ions Showing Near-Infrared to Visible Photon Upconversion", Optical Materials, 2005, 27 (5), 1111–1130.
9. Wang, F., and Liu, X., "Recent Advances in the Chemistry of Lanthanide-Doped Upconversion Nanocrystals", Chemical Society Reviews, 2009, 38 (4), 976–989.
10. Perrella, R., Ribeiro, I., Campos-Junior, P., Schiavon, M., Pecoraro, E., Ribeiro, S., and Ferrari, J., "$CaTiO_3$:Er^{3+}:Yb^{3+} Upconversion Under 980 nm and 1550 nm Excitation and its Potential as Luminescent Probes for Cells", Materials Chemistry and Physics, 2018, 223, 143–150.
11. Chen, G., Qiu, H., Prasad, P. N., and Chen, X., "Upconversion Nanoparticles: Design, Nanochemistry, and Applications in Theranostics", Chemical Reviews, 2014, 114 (10), 5161–5214.
12. Tian, L., Xu, Z., Zhao, S., Cui, Y., Liang, Z., Zhang, J., and Xu, X., "Upconversion Luminescence of Er^{3+}/Yb^{3+}/Nd^{3+} Triply-Doped β-$NaYF_4$ Nanocrystals Under 808-nm Excitation", Materials, 2014, 7, 7289–7303.
13. . Eduardo, A.C., et al. "Structural disorder-dependent upconversion in Er^{3+}/Yb^{3+}-doped calcium titanate." Ceramics International, 2014. DOI: 10.1016/j.ceramint.2014.07.127.
14. Jena, P., Kumar, D., Patro, P.K., Lenka, R.K., & Singh, A.K. "Structural characterization and electrical/electrochemical studies of $Nd_{1-x}Ba_xCo_{1-\gamma}(Fe,Ti)_\gamma O_3-\delta$ ($0 \leq x \leq 0.3$, $y = 0, 0.2$) as cathode materials for SOFC applications." Journal of Solid State Chemistry, 2020, 292, 121682.
15. Kumar, D., Prajapati, P., Jena, P., & Singh, A.K. "Size and composition dependent structural investigations on $Nd_{1-x}Ba_xCoO_3$ ($x = 0.2, 0.3, 0.4$) perovskite cobaltite using XRD." Materials Today: Proceedings, 2020, 26, 3492–3496.
16. Itoh, M., et al. "Structural phase transition from rhombohedral to cubic in $LaCoO_3$." Journal of the Physical Society of Japan, 2000, 69, 3468–3469.
17. Howard, C.J., Stokes, H.T. "Group-theoretical analysis of octahedral tilting in perovskites." Acta Crystallographica Section B: Structural Science, 1998, 54, 782–789. DOI: 10.1107/S0108768198004200.
18. Shannon, R.D. "Revised effective ionic radii and systematic studies of interatomic distances in halides and chalcogenides." Acta Crystallographica Section A, 1976, 32(5), 751–767.
19. Bai, Y., Zhou, S., Zhang, L., & Zhang, H. "Structure and photoluminescence properties of rare-earth doped $CaTiO_3$ phosphors." Journal of Alloys and Compounds, 2015, 647, 625–631.
20. Li, Y., Guo, C., Chen, B., & Yu, M. "Enhanced upconversion luminescence and structural stability in rare-earth-doped perovskite-type oxides." Ceramics International, 2018, 44(13), 15827–15834.
21. Chen, X., Xu, Y., Zhao, C., Wang, L., Wen, S., Shi, Y., Xia, Q., Shi, M., Chu, Y., Li, F., Chen, F., & Liu, K. "Activated $CaTiO_3$ phosphors via selective A-site and B-site substitution." Journal of Electronic Materials, 2020, 49(3), 1254–1263.

22. Kumar, D., Singh, A.K. "Quenching of spin–orbit coupling and Griffiths phase signatures in nanocrystalline $La_{0.6}Ba_{0.4}MnO_3$ perovskite manganite." Journal of Solid State Chemistry, 2022, 309, 122986.
23. Jo, S. K., Park, J. S., & Hane, Y. H. Effects of multi-doping of rare-earth oxides on the microstructure and dielectric properties of $BaTiO_3$. Journal of Alloys and Compounds, (2010), 501(2), 259–264.
24. Zhou, Y., Chen, D., Ji, Z., & Huang, P. "Microstructure-controlled upconversion luminescence in Yb^{3+}/Er^{3+} co-doped perovskite oxide phosphors." Optical Materials, 2019, 91, 30–38.
25. Mostafa, M. "Structural and optical properties of calcium titanate ($CaTiO_3$) prepared from gypsum." Journal of Nanotechnology, 2022, Article 4365892.
26. Mu, J., Sun, W., Li, F., Guan, Y., Zhou, X., Li, J., & Chen, L. "Upconversion luminescent perovskite $CaTiO_3:Yb^{3+}/Er^{3+}$ nanocubes." Journal of Alloys and Compounds, 2019, 797, 1002–1006.
27. Shi, R. & Mudring, A.V. "Phonon-mediated nonradiative relaxation in Ln^{3+}-doped nanocrystals." ACS Materials Letters, 2022, 4(9), 1602–1611.
28. Tripathi, N., Ghosh, P., Barman, S., & Verma, S. "Enhanced near-infrared-to-visible upconversion in $CaTiO_3:Yb^{3+}/Er^{3+}$ phosphor via host lattice modification using Mg^{2+} co-doping." RSC Advances, 2023, 13, 35391–35396.
29. Tripathi, N., Kamada, K., Nakamura, H., & Tomoko, A. "Enhanced near-infrared-to-visible upconversion in $CaTiO_3:Yb^{3+}/Er^{3+}$ phosphor via host lattice modification using Mg^{2+} co-doping." RSC Advances, 2023, 13, 35391.
30. Goethals, J., Bedidi, A., Fourdrin, C., "Experimental study of trivalent rare-earth element incorporation in $CaTiO_3$ perovskite: evidence for a new substitution mechanism." Physics and Chemistry of Minerals, 2019, 46, 1003–1015.
31. Wang, F. & Liu, X. "Recent advances in the chemistry of lanthanide-doped upconversion nanocrystals." Chemical Society Reviews, 2009, 38, 976–989.